

## INVESTIGATION OF METHYLAMMONIUM LEAD BROMIDE HYBRID PEROVSKITE BASED PHOTOACTIVE MATERIAL FOR THE PHOTOVOLTAIC APPLICATIONS

D. KUMAR<sup>a</sup>, J. CHAUDHARY<sup>b</sup>, S. KUMAR<sup>c</sup>, S. R. BHARDWAJ<sup>d</sup>,  
M. YUSUF<sup>e</sup>, A. S. VERMA<sup>e,\*</sup>

<sup>a</sup>Department of Chemical Engineering, Banasthali Vidyapith, Banasthali 304022, India

<sup>b</sup>Department of Physics, Banasthali Vidyapith, Banasthali 304022, India

<sup>c</sup>Department of Chemistry, Banasthali Vidyapith, Banasthali 304022, India

<sup>d</sup>Department of Physics, B. S. A. College, Mathura 281004, India

<sup>e</sup>Department of Natural and Applied Sciences, Glocal University, Saharanpur 247232, India

Metal halide perovskites are bringing us closer to the goal of energy self-sufficient buildings. In this paper, we have been prepared device {FTO (Fluorine-doped tin Oxide)/CH<sub>3</sub>NH<sub>3</sub>PbBr<sub>3</sub>/Spiro-OMeTAD/Al} of by using methyl amine lead bromide base as photoactive materials for the photovoltaic applications, and then investigate the parameters involved. In order to fabricate, low-temperature solution-processed devices using one-step spin coating methods play a key role in producing uniform thin films. The spin coating technique has been used for the deposition of the precursor solution including methylammonium bromide (MABr) and lead bromide (PbBr<sub>2</sub>) with molar ratio (3:1) to prepare the thin films onto FTO-substrate. The topographical studies of the thin films prepared have been done by field emission scanning electron microscopy (FESEM). Furthermore, the required parameters of the device such as; ideality factor, barrier height, saturation current, carrier mobility, current density, resistance, capacitance and carrier lifetime have been calculated by current-voltage(I-V) characteristics and Impedance Spectroscopy technique. The device was irradiated by a laser of power 20mW functioning at wavelength of 532nm. At low voltage the current conduction mechanism displays Ohmic behavior and trap free space charge limited conduction (TFSCLC) controls the charge transport at mid voltages. While trap controlled space charge limited conduction (TCSCLC) reveals at high voltages. The hole mobility has been estimated by TCSCLC model.

(Received December 1, 2020; Accepted February 13, 2021)

**Keywords:** Metal halide perovskites, Spin-coating, Charge carrier mobility, Resistance, Capacitance, Life-time, Electrochemical impedance spectroscopy

### 1. Introduction

Regardless, organic electronic devices give a reasonable path for feasible power sources and other further applications due to its easy arrangement, preparation, producing, ease of materials, and less environmental impact [1]. A lot of investigation has focused on progress of cost effective and practically possible non-silicon solar cell advancements. Due to the potential of this technology, it might be a substitute of conventional energy sources, halide perovskites have formed with stimulating efficiencies of 22.7% in the few years [2]. A progressing report has exhibited the fast improvement in power transformation from 3.8% in 2009 to 24.2% in 2019 [3]. Organic-inorganic hybrid materials based Photovoltaic cells have indicated huge perfection in a specific timeframe contrasting emphatically and existing inorganic semiconductor advancements or silicon-based technology, for example, versatility and assembling costs for formation [4]. In this manner, perovskite based optoelectronic device have drawn a novel methodology of reinvented

---

\* Corresponding author: [ajay\\_phy@rediffmail.com](mailto:ajay_phy@rediffmail.com)

efforts at improving the best efficiency [5]. The initial three-dimension perovskite emitters have been accounted for porous structure of  $\text{CH}_3\text{NH}_3\text{PbBr}_3$  nanoparticles (NPs), accordingly the scope of perovskites as emitters noticeable [6]. Thusly, the investigation on 3D perovskite emitters has seriously developed and focuses on accomplishing high proficiency in Photoluminescence and Electroluminescence [7].

There have been compensated remarkable efforts by the researcher to investigate the hole blocking material or hole transporting layer. Thusly, in this paper strappingly recommended that the electron transport materials may be inadequate to accomplish the high viability. The Spiro-OMeTAD plays an important part in blocking electrons, transport the holes, and impedance of charge recombination in perovskite-based devices. Additionally, hole transport materials are valuable to enhance the performance of perovskite-based solar cells [8-16].

Different methods have been utilized to prepare unvarying perovskite film, by using spin coating, thermal evaporation, dip coating, vapor aided methods and Spray coating [17-21]. Charge transport and resistivity both are rely on the semiconducting behavior of hybrid halide base perovskite devices, high carrier mobility and short carrier diffusion lengths. The ionic charge transport in the hybrid perovskites may show by the examinations of impedance spectroscopy [22].

The current study based on,  $\text{CH}_3\text{NH}_3\text{PbBr}_3$  is an appropriate candidate to be used as photo active layer in optoelectronics devices. In  $\text{CH}_3\text{NH}_3\text{PbBr}_3$  perovskite nanoparticles, the function of the sensitizer is to injecting elections into; electrons in the electron transport layers (ETLs) and holes in the hole transport layer (HTLs) and both the layers to be work as selective contacts throughout perovskite device which is related to charge carrier formation by photo excitation [23, 24]. Different holes transport layers (HTLs) like as PEDOT: PSS, P3HT: PCBM, and Spiro-OMeTAD have been reported. In this paper, Spiro-OMeTAD have been use as hole transport layer material, which deposited between the perovskite layer and the evaporated metal electrode. Effective masses of photo generated electrons and holes have been reported; mass of electrons ( $m_e^* = 0.23 m_0$ ) and mass of openings ( $m_h^* = 0.29 m_0$ ), respectively [25]. The materials for the transport layers are chosen with the ultimate objective that the energy barriers must anticipate the entry of holes into the Electron transport layer and electron into hole transport layer. Spiro-OMeTAD as HTL (opening vehicle layer) improves the solar cell performance [26-29].

The effective charge carrier mobility is mostly depending upon the diffusion length of the charge charier and the probability of an excited charge carrier to achieve their respective electrodes. In overall, defects in the crystal structure are probable to reduce the lifetime of photo-generated charge carriers in the device [30-32].

Impedance spectroscopy (IS) has been broadly used for the principles of organic photovoltaic devices as part of current study. In this paper, we have imparted to the essential approach to manage the examination of the impedance spectroscopy to characterize the behavior of an electrochemical structure, and therefore allow analyzing numerous phenomena inside the cell and assessing the structure losses. The optimization and further development of a new photovoltaic technology requires a deep knowledge of the working principles of this photovoltaic device [33-35].

## 2. Experimental details

### 2.1. Materials Used for Device Fabrication:

In this work, Fluorine-doped tin Oxide (FTO) deposited onto glass substrate (Sheet opposition  $\sim 8-12 \Omega/\text{cm}^2$ ), Methylamine ( $\text{CH}_3\text{NH}_2$ ), HBr and 2,2',7,7'- Tetra-kis[N,N-di(4-methoxyphenyl)amino]-9,9'- spiro-bi-fluorene (Spiro-OMeTAD) were bought from Sigma Aldrich, while dissolvable anhydrous N,N-dimethyl-formamide (DMF) and aprotic solvent diethyl ether was bought from Merck. All these materials were used as received without further purification.

### 2.2. Substrate Cleaning with Ozone Treatment:

The Fluorine-doped tin oxide (FTO) substrates was washed with cleansing soap then sequentially clean in distilled water, acetone, and 2-propanol for 15 min in an ultrasonic bath. After

that, the substrate was kept under the ultraviolet (UV) for 15 min to improve the surface control of the substrate that improved the device performance.

### 2.3. Synthesis of $\text{CH}_3\text{NH}_3\text{PbBr}_3$ perovskite precursor solution:

The synthesis process of perovskite precursor has been described schematically in the below given Fig. 1.

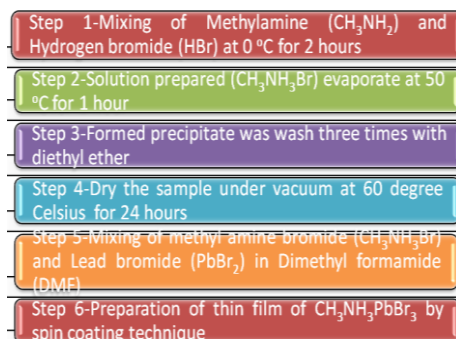
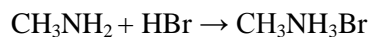


Fig. 1. Synthesis process of perovskite precursor solution by chemical route.

Following reactions are take place in the formation of methyl amine lead bromide ( $\text{CH}_3\text{NH}_3\text{PbBr}_3$ );



$\text{CH}_3\text{NH}_3\text{Br}_3$  was prepared by using methylamine ( $\text{CH}_3\text{NH}_2$ ) and HBr.  $\text{CH}_3\text{NH}_2$  was precooled to  $0^\circ\text{C}$ , under vigorous blending and HBr added to methylamine gradually after preparation of solution, it was mixed for 2 hours. At that point the solution was kept in rotatory vacuum evaporator and the prepared powder was dissolved in ethanol and wash multiple times with diethylether for precipitation and dried under vacuum. In the presence of  $\text{CH}_3\text{NH}_3\text{Br}$  and  $\text{PbBr}_2$  in (3:1) molar ration, transparent solution was acquired.  $\text{PbBr}_2$  solubility is unsurprising to be upgraded in DMF. The utilization of simple  $\text{CH}_3\text{NH}_3\text{Br}$  (MABr) can incredibly improve the nature of the perovskite film by decreasing the quantity of little crystal grains to form enormous ones, which can considerably reduce grain boundaries and empower direct connection of electron and hole transport layers with one enormous crystal grain. Before spin coating warm the solution at  $70^\circ\text{C}$  for up to 30 mints while with strong mixing, to get the reasonable transparent solution. Through the white residues in solution will be unable to get smooth film.

### 2.4. Device fabrication and characterization:

The prepared perovskite solution has been deposited onto glass-substrate by spin coating method, the crystal structure of perovskite shown in figure 2 (a), aggregate of crystal structure in figure 2 (b); while surface morphology of the prepared perovskite nanoparticles has been appeared in figure 2(c). The solution of perovskite-based device (FTO/perovskite/Spiro-OMeTAD/Al) has been showed up in figure 3 (a, b) and energy level diagram of the materials has presented in figure 3 (c) with the charge carrier transportation. Construction of perovskite-based device, firstly perovskite solution kept onto Fluorine doped oxide glass-substrate at 2000 rpm for 40 sec by one step spin coating technique to form the photon retaining layer. There after the substrate was strengthened at  $70^\circ\text{C}$  for 5 minutes.

The hole transport layer (HTL) of spiro-OMeTAD layer deposited onto active perovskite for 40 seconds by using of spin coating technique at 3000 rpm. The deposition process of has been done in glove box unit in an inert environment. As mentioned previously the hole transport layer coated over active perovskite layer which was prior coated over FTO Glass substrate and Lastly,

aluminum as electrode has been deposited onto hole transport layer with the help of thermal evaporation technique at a pressure of  $10^{-5}$  torr to form the upper electrode of the device. Currently, the additional characterization has been done of the prepared device by using distinctive measures.

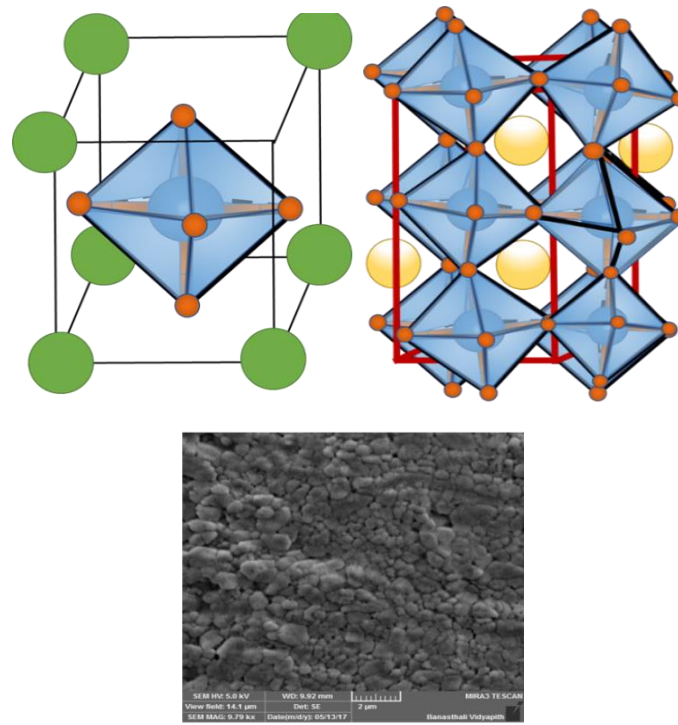


Fig. 2. Structural Morphology of perovskite (a) Crystal Structure of Perovskite, (b) Aggregate of perovskite crystal structure (c) FESEM image of  $\text{CH}_3\text{NH}_3\text{PbI}_3$  perovskite thin film.

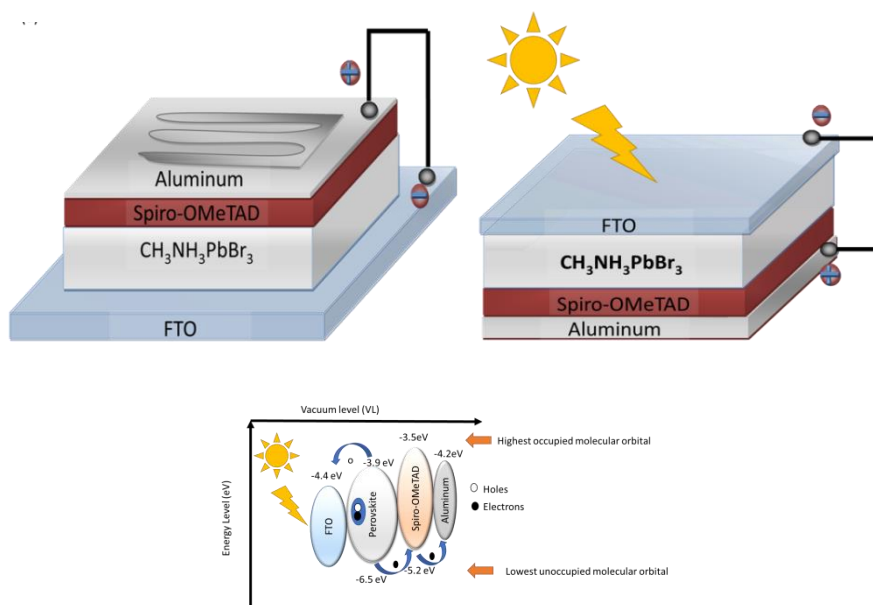


Fig. 3. (a, b) Hetero-structure of the device structure with perovskite as an active layer, (c) the energy band diagram of related device with charge transport process.

### 2.5. Characterization techniques:

The topographic of the methylammonium lead bromide thin films has obtained using FESEM (Tes-can MIRA 3 LMU FEG). The current-voltage (I-V) estimations had been grabbed with the help of a Keithley source meter 2612 appended with a manual test station (LA-100 DC, Semi-test USA). The internal electrical properties of the device have been accomplished by using electrochemical Impedance Spectroscopy basically which measures the resistance and capacitance properties of a given material/device. The impedance spectra of the device were acquired utilizing an electrochemical workstation (AUTOLabPGSTAT30) at zero voltage in the darkness. The EIS-analyzer programming was applied to fit and examine the EIS results.

## 3. Results and discussion

In this paper, we have examined about performance of methyl amine lead halide base device (FTO/ $\text{CH}_3\text{NH}_3\text{PbBr}_3$ /Spiro-OMeTAD/Al) in which  $\text{CH}_3\text{NH}_3\text{PbBr}_3$  is utilized as photoactive material. In the formation of the device quality of the film is the primarily step, which is responsible for the competent parameters of the device. A complete surface analysis of the thin film development on a FTO- Glass substrate has been revealed by field emission scanning electron microscopy (FESEM) along with the grains of the perovskite crystal; as shown in Fig. 2. we have observed from the Fig. 2 (b) the thin film of photo active perovskite ( $\text{CH}_3\text{NH}_3\text{PbBr}_3$ ) has been produced with uniform grains, complete surface coverage and negligible agglomeration

The Current-Voltage (I-V) qualities of the device have been measures under dark and light both conditions. From FTO side the device was exposed to laser light which was having intensity 20mW with the frequency of 532nm. The notable dependency of forward current, on voltage and saturated current, in reverse bias condition in darkness I-V curve shows getting better behavior of the device.

In forward bias, applied voltage brings down injection barrier for electrons and holes as appeared in the energy band diagram 3(c). The hetero structure of manufactured device has appeared in Fig. 3 (a, b) with the plausible transportation of the photo-generated charge-carrier show through the energy band diagram showed in Fig. 3 (b).

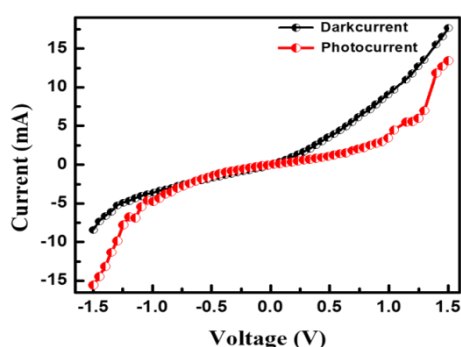


Fig. 4. I-V curve of the  $\text{CH}_3\text{NH}_3\text{PbBr}_3$  device in dark and light.

The Fig. 4 reveals the current-voltage (I-V) characteristics of the methyl amine lead bromide; which is photoactive materials, base device as represented in square bracket (FTO/ $\text{CH}_3\text{NH}_3\text{PbBr}_3$ /Spiro-OMeTAD/Al) under dark and light conditions. The current increases dramatically in both darkish and light condition, whilst the usage of forward bias of I-V curves. Even though, the energy barrier come to be low, because the internal field is equalized and bands emerge as flat so that both electrons or holes can circulate in the direction of their unique electrodes (FTO/Al). Underneath reverse bias, the chare carriers facing problems in transportation, because the Fermi level splitting and power barrier turns will become so excessive of 1.5eV at the interfaces of Al/Spiro-OMeTAD, because of excessive energy barrier, the electrons cannot circulate quickly as they travel in forward bias. This is the indication of electron blocking

interface, similarly, the high energy barrier of 2.1eV at interface of FTO/perovskite blocks the holes injection, consequently, limited current flow in the reverse direction. We have also noted that excitation of device with light lead to considerable changes in the current levels, and the current increases with increasing in the applied voltage. The excitons were generated during the illumination of device in the active-layer, and then these excitons subsequently dissociated into free charge carriers (electrons and holes), because of internally developed electric field and externally applied voltage. These free charge carriers at that point influenced by applied voltage, were moved to the concern electrodes as appeared in Fig. 3 (b), the appropriate photocurrent yields in the referenced setup (FTO/CH<sub>3</sub>NH<sub>3</sub>PbBr<sub>3</sub>/Spiro-OMeTAD/Al) as shown in Fig. 4. This plentiful increase in the photocurrent has been fundamentally attributed to the improved charge collection efficiency. The incident photons were occupied brightening in the perovskite layer, when it was exposed to light, and produced large number of excitons. These excitons eagerly separate into the free charge carrier such as holes in the valence band and electrons in the conduction band. The excited holes move to the HTL (Spiro-OMeTAD) layer/ region and then collected by the Al electrode; similarly, the electrons move to (FTO) electrode by an applied electric field. The photocurrent enhanced in the reverse bias. Still, Spiro-OMeTAD has been remains the standard Hole transport material and presented as promising material for hole transport in the perovskite-based devices, hence acquiring massive consideration in this field. However, Spiro-OMeTAD material consistently has demonstrated the reasonable matching of HOMO-LUMO levels with the perovskite material, which is contribute to enhance photocurrent in the perovskite-based devices.

The photovoltaic performance of the methyl amine lead bromide perovskite crystals has been definitely improved by the increasing temperature, under which methyl amine bromide have been dried during the synthesis of methylamine solutions, and also improve the parameters such as, saturation current (I<sub>s</sub>), hole's mobility, trap density, and barrier height and detectivity (which is responsible for progress of charge generation), carrier diffusion and charge separation in the device. The effect of structure parameters which utilized from I-V measurements of the device on photocurrent, a summary of the data is collected in Table 1.

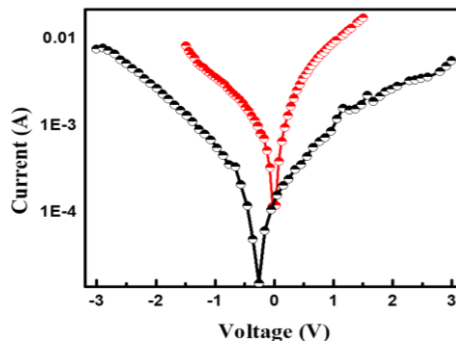


Fig. 5. I-V black curve shows semi-logarithmic curve using CH<sub>3</sub>NH<sub>3</sub>PbBr<sub>3</sub> device.

Table 1. Device paramters.

Parameters	Values
I <sub>s</sub> (Amp)-dark	4.05×10 <sup>-4</sup>
I <sub>s</sub> (Amp)-light	1.07×10 <sup>-3</sup>
Detectivity (Jones)	9.10×10 <sup>17</sup>
Φ <sub>B</sub> (Volt)-dark	0.70
Φ <sub>B</sub> (Volt)-light	0.68
μ (cm <sup>2</sup> v <sup>-1</sup> s <sup>-1</sup> )	3.1 ×10 <sup>-3</sup>
n <sub>i</sub> (cm <sup>3</sup> )	1.58×10 <sup>15</sup>

We have discovered that the device allows suitable currents in the device, as shown in the Table 1, reverse saturation current ( $I_s$ ) has been indicated by  $I_s$  that extracted utilizing Shockley diode equation [36] taking semi-logarithmic plot of I-V curve at 0 V as shown in Fig. 5:

$$I = I_s \left[ \exp\left(\frac{qV}{\eta kT}\right) - 1 \right] \quad (1)$$

Here  $q$ ,  $k$ ,  $\eta$ ,  $V$ ,  $T$ , and  $I_s$  are the electronic charge, Boltzmann's constant, ideality factor of diode, applied voltage, absolute temperature, saturation current respectively.

The ideality factor and reverse saturation current both can be measured by the slope, and intercept at y axis at 0 V, on semi-logarithmic I-V characteristics curve from the knowledge of  $I_s$ , respectively. The value close to 1 of an ideality factors demonstrating Schottky diode or an ideal diode, whereas the value of ideality factor greater than 1, which indicates that current increases more gradually in contrast with  $\eta = 1$ . High values of ideality factor of the fabricated device may increase recombination because of the presence of traps, presence of interface states and barrier in-homogeneity. Nonetheless, the boundary of Schottky diode is the barrier height ( $\phi_B$ ) that determined by following relation [37].

$$I_s = AA^*T^2 \exp\left(-\frac{q\phi_B}{kT}\right) \quad (2)$$

In above expression,  $A$  denotes to area,  $A^*$  is the Richardson's constant and  $\phi_B$  is the barrier height.

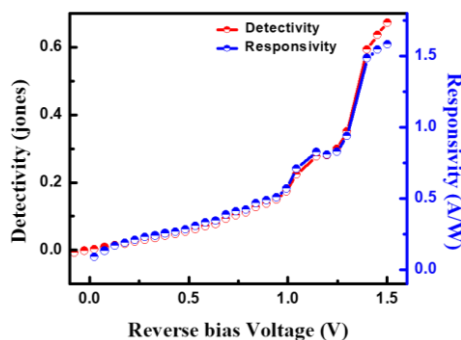


Fig. 6. Responsivity and detectivity of the fabricated device.

The photo-detector shows different significant parameters such as responsivity and detectivity. Responsivity has been determined by the ratio between the generated photocurrent ( $I_{ph}$ ) and the amount of optical power ( $P_o$ ) incident on the detector and is determined by using of following equation [38]:

$$R_p = \frac{I_{ph}}{P_o} \quad (3)$$

Here  $I_{ph}$  and  $P_o$  are the photocurrent and incident optical power respectively

Detectivity is identified with the responsivity and noise equivalent power; it estimates performance of the detector against noise [39]. Whenever shot noise is overwhelmed equivalent source in dark current, and the simple has been utilized to ascertain the estimation of detectivity [40].

$$D^* = \frac{R_p}{(2eI_D)^{1/2}} \quad (4)$$

In the equation number (4), dark current is denoted by  $I_D$ ,  $R_p$  is responsivity and  $e$  is the charge of electrons.

The features of responsivity and detectivity have been represented in Fig. 6 for the device on applied reverse voltage. Eventually, the detectivity of the device has been determined at 0V was  $9.10 \times 10^{17}$  Jones. Thus, the device appeared the suitable estimation of detectivity is due to the improvement in photocurrent. However, this incident demonstrated that the device may be a self-powered just as the device needs externally powered to identify the optical signals. In this current study, the hole transport layer expresses to the hole extracting contact at the interface between the Spiro-OMeTAD and perovskite material in planar photoactive device, which make it intensely attractive in photovoltaic group because of the powerful performance.

The topography of perovskite layer is capable to achieve the improvement in the hole's mobility. Further, three different charge transport mechanisms of device have been considered by examining the twofold logarithmic current-voltage characteristics, appeared in figure 7 and observe the overall power law dependence of  $J \propto V^m$  in which  $m$  represents to the slope of the curve.

With the observation of Fig. 7, at low voltage values, the curve begins to follow the Ohmic behavior ( $m=1$ ). From that point onward, the slope becomes ( $m=2$ ) indicating the TFSCLC mechanism governs the charge transport process of increasing voltage. Consequently, the slope has become more noteworthy than 4.85 ( $>2$ ) because of the further injection of charge carrier; which results that with applied voltage the current in this region increased gradually and follow trap charge controlled limited conduction mechanism (TCLC).

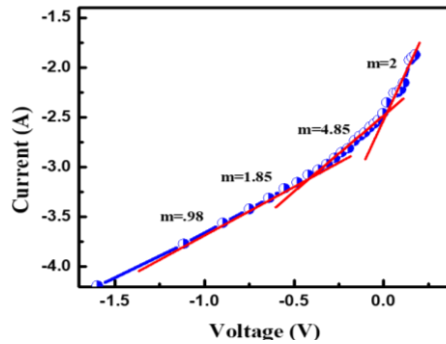


Fig. 7. Double-logarithmic plots of the devices in dark and the slope represented by  $m$  in different regions of  $CH_3NH_3PbBr_3$  perovskite-based device.

It is possible since the filled traps at higher voltage; consequently, the current is not disturbed by the traps. In this region (TFSCLC) hole's mobility ( $\mu$ ) is calculated by applying Mott-Gurney law [41].

$$J_{SCLC} = \frac{9}{8} \epsilon \epsilon_0 \mu \frac{V^2}{d^3} \quad (5)$$

where,  $\mu$  is mobility of holes,  $L$  denotes to thickness of perovskite layer,  $\epsilon$  denotes to relative dielectric constant,  $\epsilon_0$  is vacuum permittivity and  $N_T$  is trap density which is derived by following formula [42, 43].

$$V_{TFL} = \frac{e N_T L^2}{2 \epsilon \epsilon_0} \quad (6)$$

Here,  $L$  denotes to thickness of perovskite layer,  $V_{TFL}$  is the trap filled limited voltage in SCLC region,  $N_T$  is trap density,  $\epsilon$  denotes to relative dielectric constant, and  $\epsilon_0$  is vacuum permittivity.

When the voltage applied to the devices; the charge mobility, density and electric field all these parameters enhanced, although small deviations. According to Table 1, the saturation

current ( $I_s$ ) measured in dark and light from  $4.05 \times 10^{-4}$  mA to  $1.07 \times 10^{-3}$  mA in reverse bias direction. Suitably, the other parameters have been significantly improved in illumination than dark. By study of the charge transport and photoresponse of fabricated device, it has clearly demonstrated that device shows proper parameters as depicted by the figure and table.

To establish a better approach for charge transportation and interfacial charge transfer process; the experiment with impedance spectra was recorded using the Nyquist plots in Fig. 8. The model of the electrical equivalent circuit which is shown in Fig. 8 (c), provides an appropriate fit of the experimental data to remove parameters. The series and parallel resistances  $R_s$  and  $R_p$  applied to contacts, conductors and related to the interface charge transport process occur inside the devices, while CPE is used as a replacement for a capacitor in devices for better matching quality.

This is replaced by  $C_p$ , which was measured from the matched spectrum of the device. The electrical parameters measured with the fitted impedance spectra data are shown in Table 2.  $R_s$  represent recombination resistance and CPE represents the coupled chemical capacity ( $C_\mu$ ) in the manufactured device [44]. According to table 2, CPE,  $R_p$  and  $\tau_n$  values of  $CH_3NH_3PbBr_3$  material can be used as active layer than other material in the presented devices, and CPE improvement indicates easy charge transport from electrode to active layer, moreover, increment in  $\tau_n$  also specifies less frequent recombination. The electron lifetime value ( $\tau_n$ ) is measured by the following formula [45].

$$\tau_n = R \times C \quad (5)$$

where,  $R$  is the parallel resistance,  $C$  is capacitance estimated from the simulated circuit utilizing EIS analyzer software and ( $\tau_n$ ) is the life time of charge carriers' excitons from the perovskite in light condition. The features of impedance spectra at low frequency are attributed to the electronic charge transport properties, while charge recombination component contributes at high frequency.

Table 2. The extracted and estimated internal device parameters of the perovskite-based devices.

Parameter	Values
$R_s(\Omega)$	173.02
$R_p(\Omega)$	7976.2
CPE	$3.09 \times 10^{-7}$
$\tau_n(\text{Sec.})$	$2.5 \times 10^{-3}$

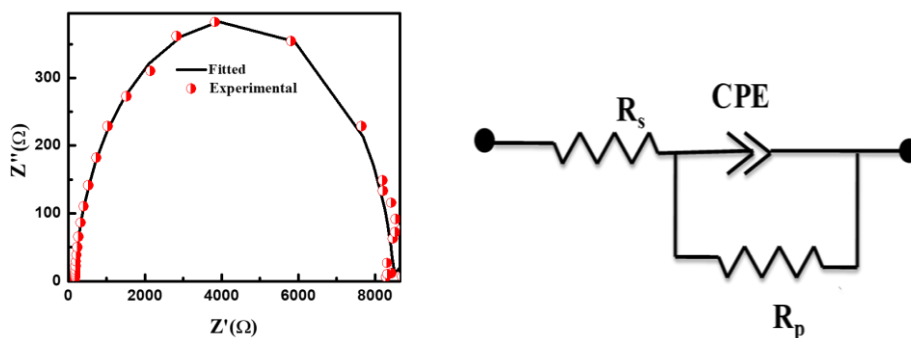


Fig. 8. (a) Nyquist plot of the working device using  $CH_3NH_3PbBr_3$ , and (b) electrical circuit diagram of the corresponding devices.

#### 4. Summary and conclusions

We have analyzed the electrical parameters of methylammonium lead bromide (FTO/CH<sub>3</sub>NH<sub>3</sub>PbBr<sub>3</sub>/Spiro-OMeTAD/Al) based device. The fabrication of the device has been done through spin coating technique, in which fluorine doped tin oxide covered glass-substrate was pretreated through ultraviolet (UV)/ozone, which contributes rise to effective charge separation and decreased recombination rates. The Spiro-OMeTAD utilize as electron blocking layer or hole transport layer between photoactive perovskite layer and top electrode for remarkable performance; and to optimize the improvement in photocurrent. The charge carrier mobility of holes has been determined by space charge limited conduction (TFSCCLC) model for the fabricated device by applying Mott-Gurney law. Besides, device has demonstrated appropriate detectivity of  $9.10 \times 10^{17}$  Jones. Successively, the electrical working of the device has been examined through I–V curve and impedance spectroscopy examination and found that CH<sub>3</sub>NH<sub>3</sub>PbBr<sub>3</sub> is suitable photoactive material for the photovoltaic device. With the sustainable proceeding with endeavors toward the development of hybrid perovskite materials, environment friendly and reliable photovoltaic innovations yielding low cost expenditure and superior will indisputably be grabbed later on around the world for applications in perovskite based photovoltaic device.

#### Acknowledgments

Corresponding author (Dr Ajay Singh Verma) is thankful to UGC-DAE Consortium of Scientific Research India, for supporting this research under the scheme of UGC-CRS (letter No. CSR/IC/BL-88/CRS-205/909).

#### References

- [1] A. K. Santhanakrishna, A. Takshi, J. Physical Chemistry C **119**(30), 17253 (2015).
- [2] M. R. Filip, G. Volonakis, F. Giustino, Hybrid halide perovskites: fundamental theory and materials design, Handbook of Materials Modeling: Applications: Current and Emerging Materials, 1 (2018).
- [3] Q. Tai, T. A. N. G. Kai-Chi, F. Yan, Energy & Environmental Science **12**(8), 2375 (2019).
- [4] S. Tombe, G. Adam, H. Heilbrunner, D. H. Apaydin, C. Ulbricht, N. S. Sariciftci, M. C. Scharber, J. Materials Chemistry C, **5**(7), 1714 (2017).
- [5] K. Chen, S. Schünemann, S. Song, H. Tüysüz, Chemical Society Reviews **47**(18), 7045–7081 (2018).
- [6] A. Cannavale, P. Cossari, G. E. Eperon, S. Colella, F. Fiorito, G. Gigli, A. Listorti, Energy & Environmental Science **9**(9), 2682 (2016).
- [7] S. T. Ha, R. Su, J. Xing, Q. Zhang, Q. Xiong, Chemical science **8**(4), 2522 (2017).
- [8] A. Mutalikdesai, S. K. Ramasesha, Resonance **22**(11), 1061 (2017).
- [9] J. Burschka, N. Pellet, S. J. Moon, R. Humphry-Baker, P. Gao, M. K. Nazeeruddin, M. Grätzel, Nature **499**(7458), 316 (2013).
- [10] H. Tan, A. Jain, O. Voznyy, X. Lan, F. P. G. De Arquer, J. Z. Fan, F. Fan, Science **355**(6326), 722–727 (2017).
- [11] G. Niu, X. Guo, L. Wang, J. Materials Chemistry A **3**(17), 8970 (2015).
- [12] J. Liu, Y. Wu, C. Qin, X. Yang, T. Yasuda, A. Islam, L. Han, Energy & Environmental Science **7**(9), 2963 (2014).
- [13] W. Ke, G. Fang, J. Wan, H. Tao, Q. Liu, L. Xiong, M. Qin, Nature Communications **6**, 6700 (2015).
- [14] L. X. Shi, Z. S. Wang, Z. Huang, W. E. Sha, H. Wang, Z. Zhou, AIP Advances **8**(2), 025312 (2018).
- [15] F. Huang, Y. Wei, L. Gu, Q. Guo, H. Xu, D. Luo, J. Wu, Energy Technology **5**(10), 1844–1851 (2015).

- [16] K. M. Boopathi, M. Ramesh, P. Perumal, Y. C. Huang, C. S. Tsao, Y. F. Chen, C. W. Chu, J. Materials Chemistry A **3**(17), 9257 (2015).
- [17] C. W. Chen, H. W. Kang, S. Y. Hsiao, P. F. Yang, K. M. Chiang, H. W. Lin, Advanced Materials **26**(38), 6647 (2014).
- [18] R. Khan, S. Javed, M. Islam, Hierarchical Nanostructures of Titanium Dioxide: Synthesis and Applications, Titanium Dioxide: Material for a Sustainable Environment, edited by Yang D., Ch. 1, 2018.
- [19] L. Zheng, Y. H. Chung, Y. Ma, L. Zhang, L. Xiao, Z. Chen, Q. Gong, Chemical communications **50**(76), 11196 (2014).
- [20] M. L. Petrus, J. Schlipf, C. Li, T. P. Gujar, N. Giesbrecht, P. Müller-Buschbaum, P. Docampo, Advanced Energy Materials, **7**(16), 1700264 (2017).
- [21] C. Eames, J. M. Frost, P. R. Barnes, B. C. O'Regan, A. Walsh, M. S. Islam, Nature communications **6**, 7497 (2015).
- [22] M. Grätzel, Nature materials, **13**(9), 838 (2014).
- [23] A. Kojima, K. Teshima, Y. Shirai, T. Miyasaka, J. American Chemical Society **131**(17), 6050 (2009).
- [24] G. Giorgi, J. I. Fujisawa, H. Segawa, K. Yamashita, J. Physical Chemistry Letters, **4**(24), 4213 (2013).
- [25] K. Mahmood, S. Sarwar, M. T. Mehran, RSC Advances **7**(28), 17044 (2017).
- [26] N. E. Courtier, G. Richardson, J. M. Foster, Applied Mathematical Modelling **63**, 329 (2018).
- [27] P. Vivo, J. K. Salunke, A. Priimagi, Materials **10**(9), 1087 (2017).
- [28] F. F. Targhi, Y. S. Jalili, F. Kanjouri, Results in Physics **10**, 616 (2018).
- [29] D. Kiermasch, P. Rieder, K. Tvingstedt, A. Baumann, V. Dyakonov, Scientific Reports **6**, 39333 (2016).
- [30] A. Guerrero, G. Garcia-Belmonte, I. Mora-Sero, J. Bisquert, Y. S. Kang, T. J. Jacobsson, A. Hagfeldt, J. Physical Chemistry C **120**(15), 8023 (2016).
- [31] F. Maddalena, P. P. Boix, C. X. Yu, N. Mathews, C. Soci, S. Mhaisalkar, Charge transport in organometal halide perovskites. In Organic-Inorganic Halide Perovskite Photovoltaics, Springer, Cham, 201 (2016).
- [32] A. Todinova, Contreras, L. Bernal, M. Salado, S. Ahmad, N. Morillo, J. Idígoras, J. A. Anta, Chem. Electro Chem. **4**(11), 2891 (2017).
- [33] H. Hu, B. Dong, W. Zhang, J. Materials Chemistry A **5**(23), 11436 (2017).
- [34] J. Chaudhary, S. Choudhary, C. M. S. Negi, S. K. Gupta, A. S. Verma, Physica Scripta **94**(10), 105821 (2019).
- [35] J. Chaudhary, S. Choudhary, C. M. S. Negi, S. K. Gupta, A. S. Verma, Semiconductors **53**(4), 489019).
- [36] K. Harada, A. G. Werner, M. Pfeiffer, C. J. Bloom, C. M. Elliott, K. Leo, Physical Review Letters **94**(3), 036601 (2005).
- [37] A. Upadhyaya, C. M. S. Negi, A. Yadav, S. K. Gupta, A. S. Verma, Superlattices and Microstructures **122**, 410 (2018).
- [38] C. H. Ji, K. T. Kim, S. Y. Oh, RSC advances **8**(15), 8302 (2018).
- [39] L. Dou, Y. M. Yang, J. You, Z. Hong, W. H. Chang, G. Li, Y. Yang, Nature communications **5**, 5404 (2014).
- [40] A. Upadhyaya, C. M. S. Negi, A. Yadav, S. K. Gupta, A. S. Verma, Semiconductor Science and Technology **33**(6), 065012 (2018).
- [41] J. Dacuña, A. Salleo, Physical Review B **84**(19), 195209 (2011).
- [42] Q. Dong, Y. Fang, Y. Shao, P. Mulligan, J. Qiu, L. Cao, J. Huang, Science **347**(6225), 967015).
- [43] Z. Zhang, W. Zheng, R. Lin, F. Huang, Royal Society open science **5**(9), 180905 (2018).
- [44] S. R. Raga, Y. Qi, J. Physical Chemistry C **120**(50), 28519 (2016).
- [45] N. Sharma, C. M. S. Negi, A. S. Verma, S. K. Gupta, J. Electronic Materials **47**(12), 7023 (2018).